Unravelling the factors that drive separation in differential mobility spectrometry: A case study of regioisomeric phosphatidylcholine adducts

Christian Ieritano,[a] J. Larry Campbell,[a,b] W. Scott Hopkins[a]*

[a] Department of Chemistry, University of Waterloo, 200 University Avenue West, Waterloo, Ontario, N2L 3G1, Canada. E-mail: shopkins@uwaterloo.ca

[b] SCIEX, 71 Four Valley Drive, Concord, Ontario, L4K 4V8, Canada.

Abstract

Differential mobility spectrometry (DMS) has shown promise as an analytical tool in the field of lipidomics. However, the underlying mechanism that drives DMS-based lipid separations is still somewhat unclear. Here, we investigate the finer details in the separability of the regioisomeric lipids 1-palmitoyl-2-oleoyl-glycero-3-phosphocholine (POPC) from 1-oleoyl-2-palmitoyl-sn-glycero-3-phosphocholine (OPPC), including the effect of cation choice, chemical modifier, and temperature. We conduct DMS-MS studies that are supported by a hybrid molecular dynamics and quantum mechanical approach to explore the conformations and energetics of the $[OPPC\cdots X]^+$ and $[POPC\cdots X]^+$ (X = Ag, K) constructs. Computational models evaluated using density functional theory reveal structural differences between low energy regioisomeric silver adducts, which translates to unique collision cross sections. Structural differences in regioisomers, as reflected through collision cross section evaluations, are not retained in potassiated adducts. Population weightings suggest coalescence of $[OPPC\cdots Ag]^+$ and $[POPC\cdots Ag]^+$ collision cross sections as higher energy species become populated at elevated temperatures. This effect presents itself experimentally, revealing diminished resolving power as the temperature of the DMS cell is increased. The results outlined here provides atomistic insight into how dynamic ion collision cross sections affect separations and guidance for future DMS-driven lipidomics applications.

Keywords: Differential Mobility Spectrometry, Mass Spectrometry, Phospholipid, Phosphatidylcholine, Collision Cross Section, Effective Temperature

1. Introduction

The lipidome of eukaryotic cells is estimated to contain up to 100 000 unique molecular entities, and as such is one of the most structurally diverse set of biomolecules.[1] While the reason for such a structural diversity eludes explanation, there is an increasing awareness for the structural significance of lipids in various aspects of homeostasis. Lipid locations and local concentrations are carefully regulated and ultimately determine structural interactions that induce specific activity. For example, a typical host cell localizes zwitterionic, neutral phospholipids, such as phosphatidylcholine (PC), to the outer leaflet of the membrane, whereas anionic phospholipids, such as phosphatidylserine (PS), exist specifically on the inner leaflet.[2,3] Owing to the role of lipids in disease epidemiology, quantitative analysis of lipids has become pivotal in the identification of biomarkers characteristic to individual ailments.

From a biological point of view, structural characterization of lipids is of particular interest owing to their functionality being strongly coupled to their structure.[4] For instance, minute variations in double bond position in one of the acyl chains of various lipids were shown to be correlated with breast cancer biomarkers[5] and adverse cardiovascular effects.[6] Given the biological prevalence of olefinic lipid components in disease, differentiation of lipids through complete structural characterization seems necessary to achieve a full mechanistic understanding.

High-throughput analysis of lipids often involves the coupling of a separation technique with mass spectrometry (MS). Liquid chromatography (LC) techniques are somewhat successful, but cannot be utilized for all lipid classes and often incorporate long run times.[7–9] More recently, techniques involving ion mobility have been prominent in lipidomics, where broad separations of lipid classes can be accomplished through differences in molecular weight and ion-neutral collision cross section (CCS).[10–

13] The application of differential mobility spectrometry (DMS) coupled to MS has also shown promise as a method to resolve isomeric and isobaric lipids.[14–20] The resolving power from DMS arises from its ability to distinguish molecular entities by their interaction potential with the carrier gas. While this property is related to the ion-neutral CCS, DMS separations also are influenced by the differential solvation incurred of unique functional groups and dynamic CCS an ion experiences as it traverses the asymmetric waveform. Numerous protocols have been developed for shotgun-driven lipidomics using DMS that rely on the direct infusion of lipid extracts and identification through MS/MS or collision induced dissociation (CID) workflows.[14,18,20] These workflows can be tuned through alteration of the carrier gas by, *e.g.,* seeding with He, which effectively alters ion mobility to enable resolution of isomeric lipids.[14,19]

The use of silver adduction towards lipidomics applications (particularly with olefinic lipids) has been well established by analogy to conventional silver ion-chromatographic approaches.[21–24] Maccarone and coworkers showed that silver cationization enables separation and quantitation of regioisomeric lipids by DMS when compared to cationization by alkali metals.[17] To this end, they were able to separate the regioisomeric pair 1-palmitoyl-2-oleoyl-glycero-3-phosphocholine (POPC; 16:0/18:1 PC) from 1-oleoyl-2-palmitoyl-sn-glycero-3-phosphocholine (OPPC; 18:1/16:0 PC) (Figure 1) through silver cationization (Figure S1). This study was followed in 2015 by Groessel and coworkers, who were able to resolve the silver adducted regioisomeric pair by high-resolution drift tube IMS.[13]

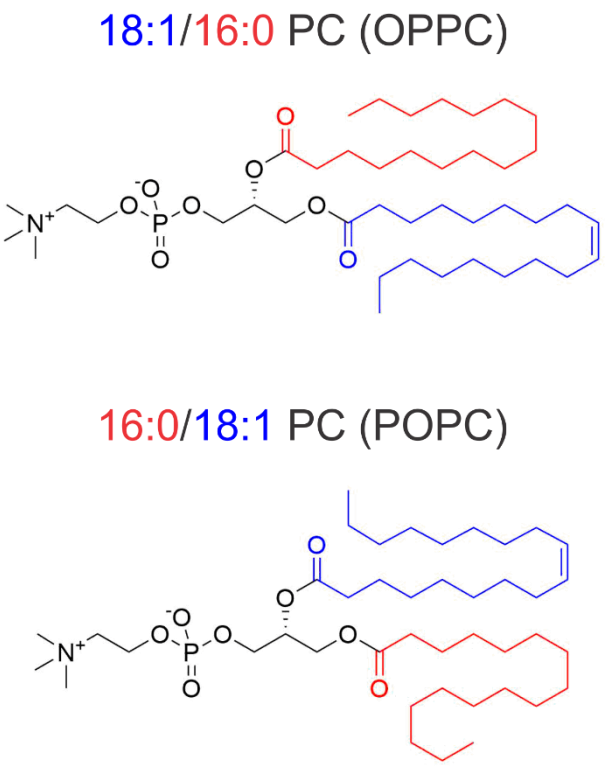

Figure 1. Structures of the regioisomeric pair 1-palmitoyl-2-oleoyl-glycero-3-phosphocholine (POPC; 16:0/18:1 PC) and 1-oleoyl-2-palmitoyl-sn-glycero-3-phosphocholine (OPPC; 18:1/16:0 PC) examined in this study.

The results from Maccarone and coworkers imply that mixtures of phospholipids, provided they contain elements of unsaturation in their acyl chains, can be easily resolved and isolated via DMS. Up until this point, justifications as to why regioisomeric lipids can be separated by DMS have been purely based on the speculation of structural changes induced by silver coordination. Here, we reinvestigate the regioisomeric pair, supporting experimental outcomes with detailed basin-hopping molecular dynamics searches of the lipid potential energy surfaces (PESs) and high-level quantum-chemical calculations of the adducts formed between OPPC and POPC with Ag and K. Theoretical CCSs are evaluated for each calculated isomer and compared with experiment in an effort to determine factors that influence separation of the lipid adducts.

2. Methods

2.1 Experimental Details

A SelexION differential mobility spectrometer was mounted in the atmospheric region of a QTRAP 5500 system (SCIEX; Concord, ON) between the sampling orifice and electrospray ionization (ESI) source. This instrumental setup has been extensively described elsewhere.[25–28] The ESI probe was operated at 5500 V, using a source temperature of 100 °C, a nebulizing gas pressure of 30 psi, and an auxiliary gas pressure of 10 psi. The DMS cell was held at fixed temperatures pertaining to the experiment of interest. N_2 was used as both the curtain gas (20 psi) and as the collision partner (*ca.* 9 mTorr) for sample acquisition in the MS^2 (Enhanced Product Ion) mode.

Synthetic PCs (POPC and OPPC) were obtained from Avanti Polar Lipids Inc. (Alabaster, AL), and diluted to working concentrations of *ca*. 0.1 µM in MeOH containing *ca*. 50 µM of the respective metal cation (also in MeOH). Silver acetate, potassium nitrate, sodium nitrate, lithium nitrate, and methanol were obtained from Sigma Aldrich (Oakville, ON, Canada) and used without further purification. Analyte solutions were infused into the ESI source at 15 µL min^{-1}.

Typically, the DMS was operated at an optimal, fixed separation voltage (SV = 4100 V), while the compensation voltage (CV) was scanned from 0 to 25 V in increments of 0.05 or 0.1 V to produce an ionogram. Data acquisition for each lipid adduct was conducted in a pure N_2 environment, in addition to DMS environments seeded with 1.5 % (mole ratio) of various chemical modifiers. The standard residence time for PC ions within the DMS cell (*ca.* 7 ms) could be tuned by application of an impeding gas flow (throttle gas) from the DMS cell terminus to enhance resolution.[25]

2.2 Potential energy surface mapping

To capture the potential energy landscape of each lipid adduct, several metal coordination schemes were considered. Molecular conformers that exhibit diverse binding motifs involving the Lewis basic carbonyl/phosphate oxygens and double bond in the oleyl side chain were generated and explored using a custom-written basin-hopping (BH)[27–33] routine interfaced with Gaussian 16.[34] Each of the $[OPPC\cdots M]^+$ and $[POPC\cdots M]^+$ (M = Ag, K) adducts were investigated computationally. Ionic species in each BH routine were modelled using the AMBER molecular mechanics force field,[35] which used partial charges for an optimized "guess structure" determined at the B3LYP/6-31+G(d,p) level of theory using the ChelpG partition scheme.[36–38]

For each structural perturbation, dihedral angles of the phospholipid head group, glycerol backbone, and acyl side chains were assigned a random rotation of $-3° < \phi < 3°$. In total, *ca*. 20 000 structures were sampled by the BH algorithm, which identified hundreds of unique conformations of each lipid adduct. Using chemical intuition and hierarchal clustering routines to sort geometries by comparison of cosine distances,[39–41] unique isomers identified by the BH routine were pre-optimized at the B3LYP/6-31G level of theory. Unique isomers generated from the pre-optimization were carried forward for full treatment at the B3LYP/6-31+G(d,p) level of theory, which has shown success in previous computational lipid investigations.[42] DFT calculations included the GD3 empirical correction for dispersion.[43] Silver was treated with the Def2-TZVP basis set and effective core potential.[44,45] Normal mode analyses were conducted to verify that each isomer corresponded to a minimum on the PES. This also served to calculate the gas-phase thermochemistry for each structure, which was used in the ordering of the Gibbs-corrected electronic energies of each unique conformer. Atomic partial charges were generated according to the Merz-Singh-Kollman (MK) partition scheme,[46,47] and constrained to reproduce the dipole moment of the isomer. All isomers were carried forward to obtain theoretical CCSs in N_2 using the MobCal-MPI package.[48] Molecular graphics were generated using the UCSF Chimera package. Chimera is developed by the Resource for Biocomputing, Visualization, and Informatics at the University of California, San

Francisco (supported by NIGMS P41-GM103311).[49] Geometries for calculated isomers are provided in the supporting information.

2.3 CCS Calculations

Collision cross sections with nitrogen (Ω_{N2}) were evaluated using the trajectory method.[50] Calculations were conducted using MobCal-MPI, a parallelized CCS calculation package developed by our group.[48] Briefly, MobCal-MPI describes van der Waals (vdW) potentials using parameterized sets from molecular mechanics forcefields, namely MMFF94, enabling distinction of unique atom types (*e.g.,* H bonded to O versus C). Since Ag^+ is not included in MMFF94, and there is an insufficient literature precedent of ion mobility studies of silver cationized species to parameterize vdW interactions for Ag^+, the Cu^+ vdW parameters were used in its place with the mass of ^{107}Ag. This should serve as a decent approximation considering the similarities in vdW radii and atomic polarizabilities for Ag^+ and Cu^+, which are used to derive MMFF94 vdW parameters (Table S1). Also note that the metal cation is effectively buried within the lipid core and should not have as large an effect as the exposed surface atoms in determining N_2 trajectories.

All CCS calculations employed 10 complete cycles of mobility calculations that used 48 points of velocity integration and 1008 points of impact parameter integration. Calculated Ω_{N2} are reported as average values with statistical errors assessed from the 10 cycles of calculation. Ω_{N2} for each lipid adduct is reported as a Boltzmann-weighted CCS based on the relative energies of the conformers (standard Gibbs energies), unless specified otherwise. The total error for a corresponding Boltzmann-weighted CCS is calculated from weighting the standard error of each CCS evaluation to the isomer relative energy.

3. Results and Discussion

3.1 Metal coordination enables resolution of isomeric PCs

To explore the effect of cation choice on separation of the regioisomeric PC pair, we reinvestigated numerous adducts of the form $[M + X]^+$ (X = H, Ag, Li, Na, and K). Ionograms of 1:1 mixtures of the PC regioisomers coordinated with the specific cation are shown in Figure 2. As expected, the regioisomeric pair is resolved when coordinated to Ag^+ with a resolving gas pressure of 30 psi, which follows the original observation by Maccarone and coworkers.[17] Detection of the lipids as protonated species $[PC\cdots H]^+$ or as adducts in a DMS cell seeded with various chemical modifiers yields no regioisomer resolution (Figures S2 and S3). In N_2, however, the Li^+ adducts exhibit some degree of separation. It should be noted that partial resolution of the Li^+ adducts required much harsher resolving gas pressures (45 psi) that resulted in significant signal depletion. This partial resolution can be understood in terms of the isomers present in the gas-phase ensemble, as Li^+ coordinated species likely resemble the population of silver adducted species based on similarities in van der Waals radii (Table S1). Given the known ability of silver to covalently coordinate olefinic moieties, this interaction likely drives a more pronounced structural difference between the regioisomers, enhancing their separation compared to Li^+ coordination. In the case of Na^+ and K^+ coordination, no isomeric resolution was observed at either 30 or 45 psi. A non-lipid contaminant (Figure 2D, blue trace) was identified in the case of K^+ coordination (*vide infra*).

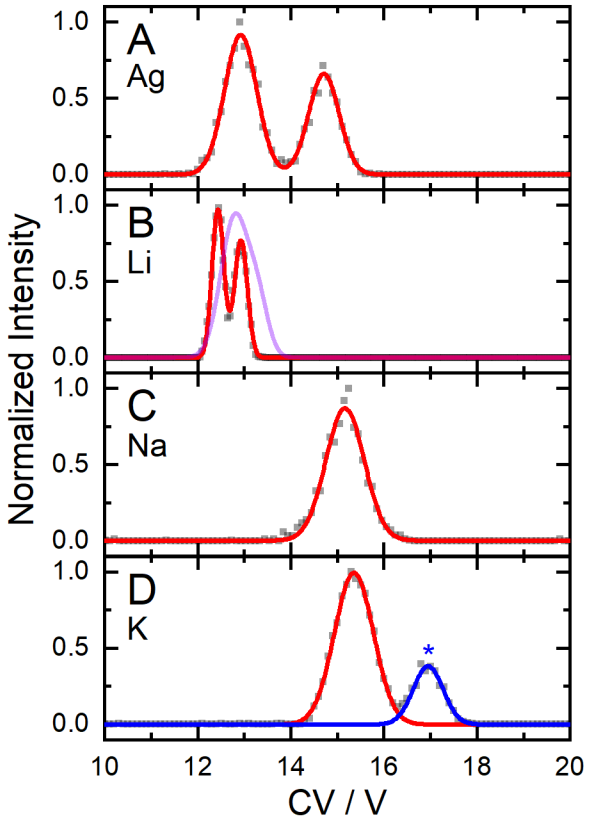

Figure 2. Total ionograms resulting from analysis of a 1:1 mixture of POPC and OPPC cationized with (**A**) Ag^+, (**B**) Li^+, (**C**) Na^+, and (**D**) K^+. All ionograms were acquired at a cell temperature of 225 °C. **A**, **C,** and **D** were acquired at SV = 4100 V with a resolving gas pressure of 30 psi. **B** was acquired at SV = 4000 V with a resolving gas pressure of 45 psi (solid red) and 30 psi (transparent purple). The blue trace in D corresponds to an unidentified contaminant in the lipid sample (see Figures S8 – S11). Raw ionogram points are shown as grey boxes.

3.2 Molecular classification of lipid adducts

To rationalize the DMS behaviour exhibited by the PC adducts, two representative cases that highlight the differences in coordination interactions were selected to not overburden computational resources. We chose to explore $[OPPC\cdots X]^+$ and $[POPC\cdots X]^+$ (X = Ag, K) given the vastly different nature of interactions

between silver/potassium to heteroatoms and olefins. Specifically, covalent interactions in Ag^+ adducts are expected as opposed to the purely electrostatic or quadrupolar interactions in K^+ adducts.

For each representative case, the choice of lipid conformation upon metal cation adduction is crucial to identify low-energy binding motifs that optimize interactions with the metal of interest. Our search of the PESs for the various lipid adducts identified numerous binding motifs, which are summarized in Figure 3. As anticipated from chemical intuition, observed binding motifs for the lipid constructs involve cation coordination through the phosphate (PO_4), acyl carbonyl oxygen found on either C1 or C2 of the glycerol backbone, and/or the double bond (DB) of the oleyl side chain. Variation in motif energetics arise with differing interaction potentials between the cations (*i.e.,* Ag^+ versus K^+) and geometric arrangements of the acyl chains.

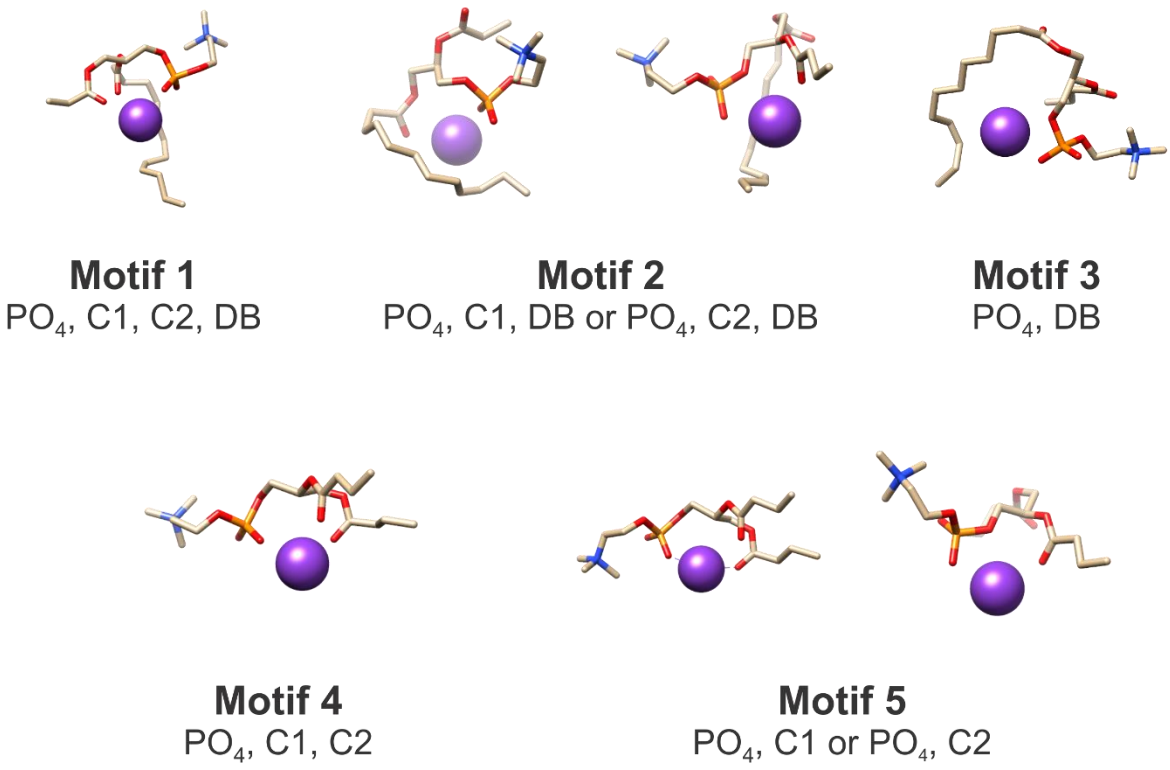

Figure 3. Binding motifs of $[OPPC\cdots M]^+$ and $[POPC\cdots M]^+$ (M = Ag, K). Acyl chains have been truncated for ease of visibility.

3.3 Structural characterization of [OPPC···X]⁺ and [POPC···X]⁺ (X = Ag, K)

Figure 4 shows the four lowest energy isomers of both [OPPC···Ag]⁺ and [POPC···Ag]⁺. Isomers are numbered in order of increasing energy relative to the global minimum. Since the regioisomeric adducts have identical chemical compositions, we paid careful attention to the conformations adopted by the headgroups and acyl chains considering that most low energy isomers fall within motifs 1 and 2. Upon examination of the low energy geometries, we firstly note the presence of a C–H···O interaction between the choline head group and either the phosphate oxygen (common in motif 1) or C1/C2 carbonyl oxygen (common in motif 2). This feature presents itself in most low energy conformers and is consistent with geometric parameters of the PC headgroup observed in methylphosphocholine and the di-palmitoylphosphocholine (DPPC).[51–53] Thus, structural differences in regioisomers likely arise from unique lipid tail orientations.

Given the asymmetry of the chain lengths (16 carbon for palmitoyl, 18 carbon for oleyl), one might expect that regioisomers that adopt identical binding motifs exhibit dissimilar acyl chain orientations upon cation coordination. For silver adducted species, this rationale makes sense owing to the covalent nature of the Ag-olefinic interaction. Since the regioisomer lipid constructs have the oleyl side chain at different starting points along the glycerol backbone (C1 for OPPC, C2 for POPC), there should be an asymmetry in the protrusion of the lipid tails. Indeed, upon examination of the calculated structures, the asymmetry is immediately obvious, where protrusion of the palmitoyl acyl chain in OPPC extends further than that of POPC. This effect induced by silver coordination gives way to OPPC exhibiting a larger CCS compared to POPC, which is supported by IMS studies (*vide infra*).[13]

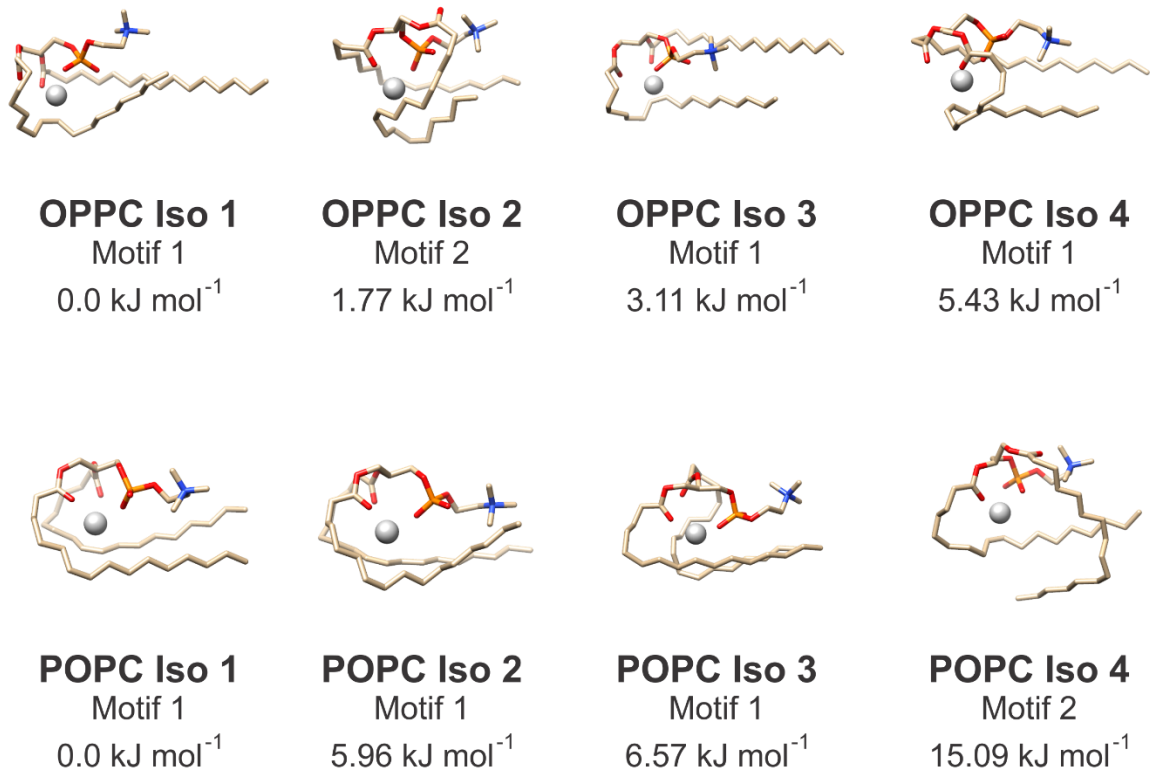

Figure 4. Calculated structures of $[OPPC\cdots Ag]^+$ (top) and $[POPC\cdots Ag]^+$ (bottom). Calculations were performed at the B3LYP/6-31+G(d,p) level of theory. The Def2TZVP basis set and pseudopotential was used for Ag. Standard Gibbs energies are reported.

The optimized structures of the four lowest energy isomers of $[OPPC\cdots K]^+$ and $[POPC\cdots K]^+$ are shown in Figure 5. Isomers are numbered in order of increasing energy from the global minimum. Following a similar geometric analysis to the silver adducted species, we considered the orientations of both the headgroups and acyl chains since Motif 1 (and Motif 2 to a lesser extent) is a common proponent of the potassiated lipid adducts.

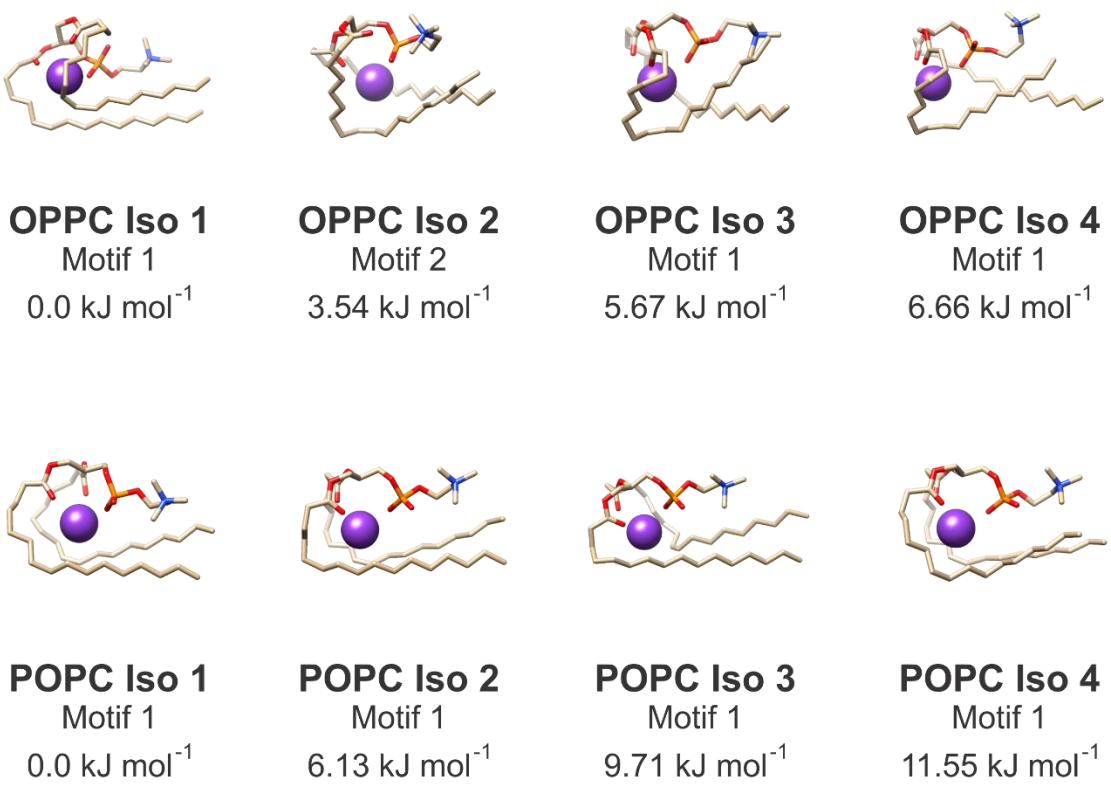

Figure 5. Calculated structures of $[OPPC\cdots K]^+$ (top) and $[POPC\cdots K]^+$ (bottom). Calculations were performed at the B3LYP/6-31+G(d,p) level of theory. Standard Gibbs energies are reported.

Upon inspection, the C–H···O interaction between the choline head group and either the phosphate oxygen or C1/C2 carbonyl oxygen is retained in nearly all low energy isomers. In fact, similar compact lipid tail organization ensembles are observed in the case of both silver and potassium adduction. Despite the nearly identical chemical composition of silver and potassium adducts, the asymmetric orientation of the acyl chains is lost in the latter coordination scheme compared to the structures of the regioisomeric silver adducts. This is likely owing to: (1) the hardness of Ag^+ relative to K^+; (2) the ability of Ag^+ to bind not only to Lewis basic sites on heteroatoms but also to olefinic π-electrons; and (3) the covalent nature of Lewis-basic–Ag^+ interactions compared to the purely electrostatic interactions between identical sites and K^+. These factors collectively increase the interatomic distances between electron rich sites with K^+ relative to Ag^+, resulting in slightly larger cation coordination cavities, and thus, a loss of asymmetric chain

organization. This logic allows a preliminary rationalization of the decreased resolution as the hardness of the alkali cation it is coordinated to increases, since a decrease in the binding cavity size should enable asymmetric tail organizations as was observed with silver adduction.

3.4 Assessing the degree of organization of lipid constructs

To investigate the asymmetry driven by cavity size and olefinic coordination to the cation observed in calculated isomers, we conducted additional calculations to sample both symmetric and asymmetric arrangements of the acyl chains. In the case of silver adducts, OPPC isomers with symmetric arrangements of acyl chains were found to be higher in energy by *ca.* 12 – 15 kJ mol^{-1} (*e.g.,* Iso 9, 13, 14, 15). In the case of POPC, asymmetric arrangements of acyl chains were found to be significantly higher in energy by *ca*. 23 kJ mol^{-1} (*e.g.,* Iso 7, 8). For potassiated lipid constructs, the onset of isomers which exhibit asymmetry in acyl chain orientations occur at similar energies. Asymmetric tail assemblies were found to be at least 10 kJ mol^{-1} (*e.g.,* Iso 8, 9) higher in energy for [OPPC···K]$^+$, and 17 kJ mol^{-1} (*e.g.,* Iso 8, 13, 16, 18) higher in energy for [POPC···K]$^+$. This suggests that the binding cavity size of the lipid constructs and the resulting asymmetry of the acyl chains adopted upon coordination of a specific cation is the driving force behind subtle structural changes enabling regioisomeric resolution by ion mobility experiments.[13] This follows the asymmetry observed in regioisomeric PCs that are not coordinated to metal cations.[54]

To confirm the preferred, compact conformations of lipid acyl chains, we enabled the BH search to explore both closely packed and separated acyl chain orientations. A comparison of the distance of closest contact between the terminal carbon of one acyl chain and any carbon of the other is provided in Figure S4. Results indicate that low energy isomers prefer closely packed geometries rather than widely separated acyl chain orientations. This is consistent with CCS calculations, where we found that an increase in isomer energy correlates with both an increase in calculated CCS and partial charge experienced by the cationic metal (Figure S5).

3.5 Theoretical collision cross section predictions of lipid adducts and relation to expected differential mobility

Boltzmann-weighted CCSs (T = 298 K) for each lipid adduct, as determined by MobCal-MPI, are summarized in Table 1. Calculated CCSs upon silver adduction are well separated for regioisomeric adducts (1.8% difference) when compared to potassium adduction (0.3% difference), and agree with IMS measurements.[13] Despite the slight underestimation of experimental CCS for the $[PC\cdots K]^+$ regioisomers, MobCal-MPI predicts the correct CCS ordering in terms of size for both pairs of $[PC\cdots K]^+$ and $[PC\cdots Ag]^+$ regioisomers.

Species	Expt. CCS / Å² (Ref. 13)	Calc. CCS / Å²	Abs error / %
$[OPPC\cdots Ag]^+$	294.7	293.2	0.52
$[POPC\cdots Ag]^+$	292.5	287.9	1.56
$[OPPC\cdots K]^+$	299.4	287.6	3.94
$[POPC\cdots K]^+$	299.9	288.4	3.83

Table 1. Comparison of Boltzmann-weighted CCSs (T = 298 K) of $[OPPC\cdots X]^+$ and $[POPC\cdots X]^+$ (X = Ag, K) as predicted by MobCal-MPI to experimental, field-corrected CCSs as determined by Groessl and coworkers (Ref 13).

However, to rationalize separations, it is necessary to consider that an ion's CCS is dynamic as it traverses the oscillating electric field. Owing to the effects of field-induced heating, it becomes difficult to evaluate the effective temperature experienced by an ion (and thus, a Boltzmann thermal population) at different points during the DMS separation. In a purely N_2 environment, one could rationalize the differential mobility incurred throughout the asymmetric waveform by an examination of isomeric contributions to the entire gas-phase population as a function of temperature. Of course, this analysis should involve a determination of isomer thermochemistry as a function of temperature. This facilitates a more representative evaluation of thermochemistry to use in Boltzmann-weighted population analyses as defined by relative Gibbs energies. However, with the dynamic heating and cooling that occurs throughout the SV waveform, this analysis becomes quickly convoluted as an ion's effective temperature (and thus,

CCS) is never static. Thus, we generalize isomer thermochemistry with standard Gibbs energies, and treat isomer CCSs as a dynamic entity that fluctuates thermally. The contribution of individual isomers to the total ensemble population as a function of temperature and CCS is shown in Figure 6.

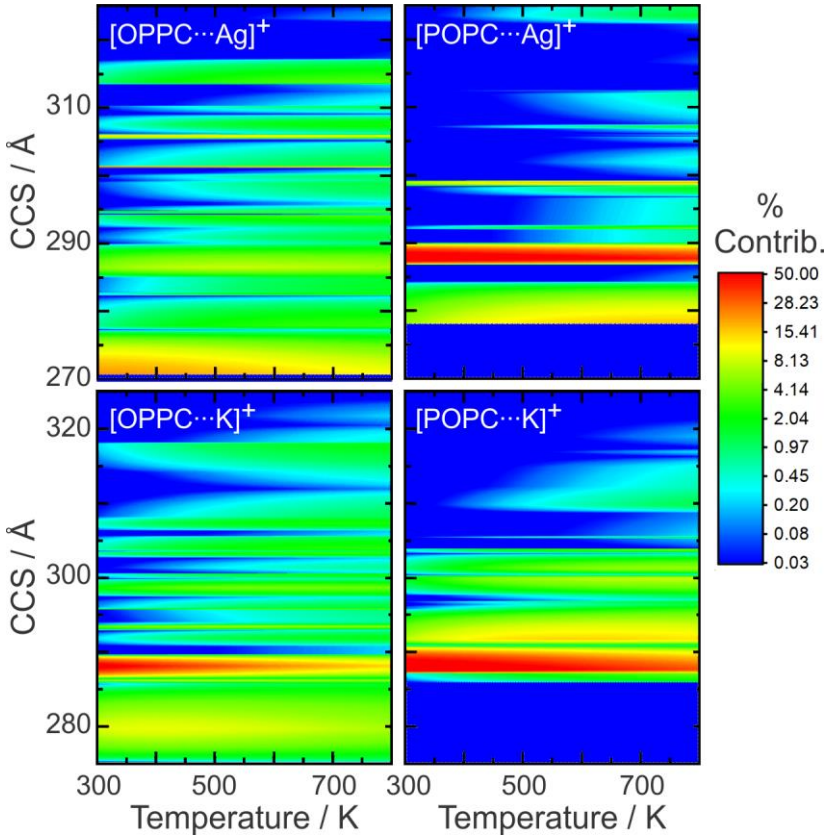

Figure 6. Relative isomer contributions to the ensemble as a function of temperature and CCS based on calculated standard Gibbs energies.

Analysis of isomer CCS as a function of temperature provides insight into the differential mobility incurred between silver versus potassium adducted PCs. $[POPC\cdots Ag]^+$ isomer relative populations are predominantly associated with species exhibiting CCSs of *ca.* 288 and 298 $Å^2$ at most temperatures sampled. In contrast, $[OPPC\cdots Ag]^+$ has several low energy isomers with larger CCSs that become populated as effective ion temperature increases. We would expect that $[OPPC\cdots Ag]^+$ exhibits the larger differential mobility as it traverses the oscillating electric field in N_2, owing to its greater change in CCS.

While silver adduction yields unique low energy geometries (*viz.* CCS) for the regioisomeric pair, coordination to K^+ seems to favour one major conformation for both PC isomers. This effect can be seen in the contour CCS contour plots of $[OPPC\cdots K]^+$ and $[POPC\cdots K]^+$, where a high density of isomers have CCSs of *ca.* 288 $Å^2$. Moreover, as ion internal energy increases, higher energy isomers of similar CCS are being populated in both $[OPPC\cdots K]^+$ and $[POPC\cdots K]^+$. Thus, we would expect both potassiated adducts to exhibit nearly identical differential mobilities in N_2, which follow the inability of DMS to resolve the regioisomeric PCs.

3.6 Temperature Dependence of Lipid Adduct Separability

The Boltzmann-weighted CCS as a function of temperature is shown in Figure 6. It becomes necessary to consider the temperature dependence of an ensemble's average CCS since population weightings change as a result of field-induced heating. Across the 300 – 800 K temperature range, the population-weighted CCSs of the silver adducted regioisomeric pairs are distinct, whereas potassium adducted pairs exhibit essentially identical CCSs at all temperatures sampled. Based on calculations, higher temperatures favour lipid conformations that exhibit less densely packed acyl chains. This raises an interesting question on the temperature dependence of the separation between on the lipid adducts. If our structural hypothesis is correct, resolution of silver adducted PCs should diminish as temperatures in the DMS cell increase.

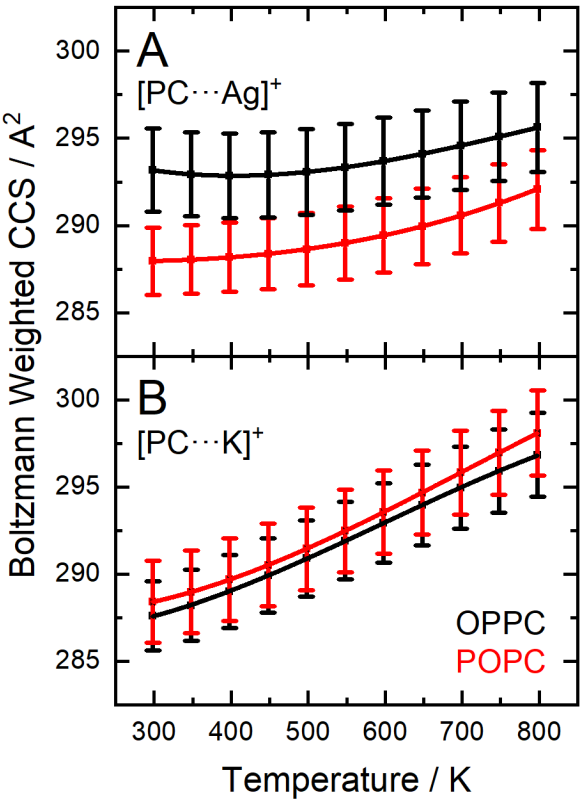

Figure 7. Boltzmann-weighted CCSs for $[PC\cdots Ag]^+$ (**A**) and $[PC\cdots K]^+$ (**B**) adducts as a function of temperature. OPPC is shown in black, and POPC is shown in red. Errors bars represent the weighted standard deviation (2σ) of the MobCal-MPI CCS calculation for all isomers.

The influence of temperature on an ion's trajectory will correlate strongly with the dynamic structural changes that occur throughout the course of the asymmetric waveform. Ultimately, changes in resolution stem from changes in the asymmetry parameter (α) that governs the mobility difference exhibited by an ion under low and high field. The α parameter strongly depends on the clustering propensity of an ion to either residual solvent from the ESI process or added as a chemical modifier, and the ion's average CCS, which is temperature dependent.[26,55] Thus, varying temperature can either enhance or diminish resolving power depending on its effect on dynamic clustering with solvent and/or average CCS.

To this end, we investigated the temperature dependence on the separation of $[OPPC\cdots Ag]^+$ and $[POPC\cdots Ag]^+$. Figures S6 and S7 show ionograms and peak widths taken at SV = 4100 V at various DMS cell temperatures using a resolving gas pressure of 30 psi. Eight scans were summed at each CV step. Raw ionograms were fit with two gaussian distributions corresponding to the two isomer peaks. Resolution (R), as defined by equation 1, is determined from the gaussian fit parameters (peak centroid and FWHM), and averaged across three independent trials. Figure 8A shows the dependence of resolution as a function of temperature for $[OPPC\cdots Ag]^+$ and $[POPC\cdots Ag]^+$. Errors are reported as the standard deviation between triplicate runs (2σ).

$$R = \frac{CV_2 - CV_1}{\frac{1}{2}(W_1 + W_2)} \quad (1)$$

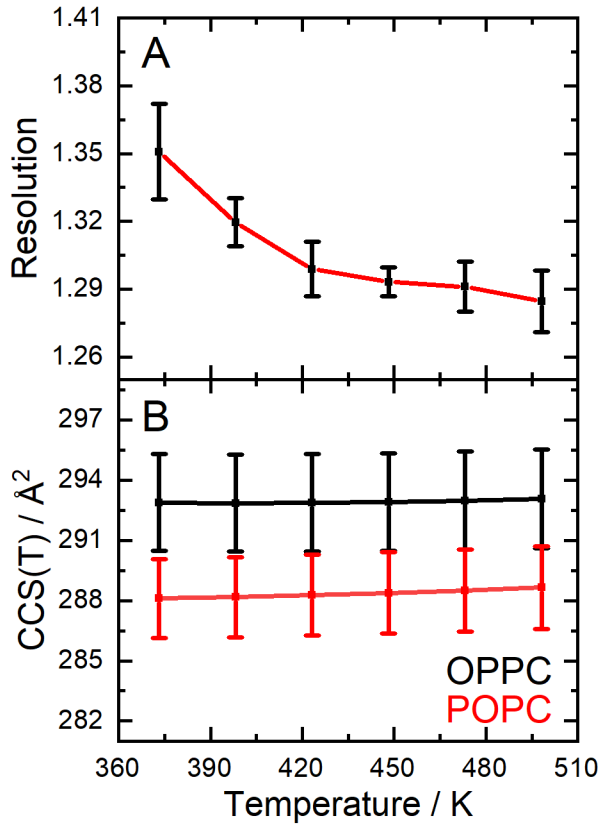

Figure 8. (**A**) Average peak resolution and (**B**) Boltzmann-weighted CCS as a function of DMS cell temperature for $[OPPC\cdots Ag]^+$ and $[POPC\cdots Ag]^+$. Error bars in **A** represent 2σ across three independent data

acquisitions. Errors bars in **B** represent the weighted standard deviation (2σ) of the MobCal-MPI CCS calculation for all isomers.

Clearly, a diminishing trend in resolution is observed as the base temperature of the DMS cell increases. Although this decrease is not substantial, one must again consider the dynamic behaviour of the gas-phase ensemble at a particular temperature. Under N_2, the predominant effect of temperature on DMS resolution stems from field-induced heating that will influence an ion's average CCS, which is temperature dependent.[55] Figure 8B shows the change in Boltzmann-weighted CCS as a function of the base DMS cell temperature. At lower temperatures, the greater difference between calculated CCSs for each regioisomer translates to enhanced resolution. As thermal energy increases, however, population of higher energy species causes the CCS of each regioisomer to coalesce, resulting in decreased resolution.

In consideration of the potassium adducts, one would expect no change in resolution as the temperature in the DMS cell is varied owing to the nearly identical Boltzmann-weighted CCSs at all accessible temperatures. Figure S8 shows that $[OPPC\cdots K]^+$ cannot be resolved from $[POPC\cdots K]^+$ at any temperature. Interestingly, the onset of an unidentified contaminant with a nominal mass nearly identical to that of $[PC\cdots K]^+$ (798.2 *versus* 798.5, respectively) emerges (with increasing resolution) as the temperature of the DMS cell increases. As evidenced through parent mass comparison and fragmentation analysis through CID experiments (Figures S9, S10, and S11), this compound is not a glycerophospholipid. Thus, while we demonstrate that DMS resolution improves with decreasing temperature for the $[OPPC\cdots Ag]^+$ and $[POPC\cdots Ag]^+$ complexes, the behaviour of the nearly isobaric contaminant demonstrates that, in some cases, resolution can improve with increasing DMS cell temperature.

4. Conclusions

In this work, we provide physical insight into the geometries adopted by $[POPC\cdots X]^+$ and $[OPPC\cdots X]^+$ (X = Ag, K) as determined by DFT. The results clearly show preferential coordination of both cations by the phosphate, carbonyl, and olefinic moieties. Interactions with the silver cation are more pronounced compared to potassium, owing to the well-known ability of silver to bind heteroatomic lone pairs and π-electrons in a covalent nature (as opposed to electrostatic). These interactions result in subtle structural differences between $[OPPC\cdots Ag]^+$ and $[POPC\cdots Ag]^+$ that ultimately facilitates their separation.

An ion's effective temperature is a crucial component in designing and/or rationalizing DMS separations. The asymmetric field utilized in DMS creates a dynamic temperature environment, which means that an ion's geometry is never static. In this case study, field-induced heating drives substantial changes in PC adduct geometry (*viz.* CCS calculations). However, separation between chemical entities (in this case, PC regioisomers) relies on populating isomerically distinct geometries as thermal energy increases. Owing to the covalent nature of Ag^+ interactions (particularly to olefins), separation of the adducted PCs is possible. This hypothesis is supported by parallel investigations of similar regioisomeric PCs.[17] Fully saturated acyl chains PC regioisomers (ie. PC (16:0/18:0) and PC (18:0/16:0)) showed no separation by DMS upon silver cationization, while those containing at least one degree of unsaturation (namely PC (18:1/18:0) and PC (18:2/16:0) along with their regioisomeric counterparts) could be separated using DMS.

Overall, the results reveal the interplay between isomer contributions to the gas-phase ensemble population and the temperature dependence of separation, where enhanced resolution of the Ag^+ adducted regioisomers is observed at lower DMS temperatures. Within the scope of lipids studied here, it is probable that similar regioisomeric lipid adducts can be well separated by DMS, provided that they contain at least one degree of unsaturation in the acyl chain. The results provide an enticing avenue for targeted separations of polyunsaturated fatty acids (PUFAs), which are prime candidates for silver

adduction owing to their high degree of unsaturation. We maintain that the study and resolution of silver adducted lipids is an attractive avenue to lipidomics across all ion mobility platforms, especially considering the enhanced resolution observed at lower instrument operating temperatures.

Acknowledgements

We gratefully acknowledge the high-performance computing support from the SHARCNET consortium of Compute Canada. The authors would like to acknowledge the financial support provided by the Natural Sciences and Engineering Research Council (NSERC) of Canada and the Ontario Early Researcher Award.

Conflicts of Interest

The authors declare that there are no conflicts of interest.

Appendix A. Supplementary data

Supplementary data associated with this article, as described in the text, can be found at http://dx.doi.org/10.1016/j/ijms.20XX.XX.XXX.

References

[1] M.R. Wenk, Lipidomics: New tools and applications, Cell. 143 (2010) 888–895. doi:10.1016/j.cell.2010.11.033.

[2] B. Fadeel, D. Xue, The ins and outs of phospholipid asymmetry in the plasma membrane: roles in health and disease., Crit. Rev. Biochem. Mol. Biol. 44 (2009) 264–277. doi:10.1080/10409230903193307.

[3] R.J. Boohaker, M.W. Lee, P. Vishnubhotla, J.M. Perez, A.R. Khaled, The Use of Therapeutic Peptides to Target and to Kill Cancer Cells, Curr. Med. Chem. 19 (2012) 3794–3804. doi:10.2174/092986712801661004.

[4] R.W. Gross, X. Han, Lipidomics at the interface of structure and function in systems biology, Chem. Biol. 18 (2011) 284–291. doi:10.1016/j.chembiol.2011.01.014.

[5] X. Ma, L. Chong, R. Tian, R. Shi, T.Y. Hu, Z. Ouyang, Y. Xia, Identification and quantitation of lipid C = C location isomers: A shotgun lipidomics approach enabled by photochemical reaction, (2016). doi:10.1073/pnas.1523356113.

[6] K. Ekroos, Lipidomics: Technologies and Applications, Wiley, New York, 2012.

[7] S. Granafei, I. Losito, F. Palmisano, T.R.I. Cataldi, Identification of isobaric lyso-phosphatidylcholines in lipid extracts of gilthead sea bream (Sparus aurata) fillets by hydrophilic interaction liquid chromatography coupled to high-resolution Fourier-transform mass spectrometry, Anal. Bioanal. Chem. 407 (2015) 6391–6404. doi:10.1007/s00216-015-8671-9.

[8] A. Anesi, G. Guella, A fast liquid chromatography-mass Spectrometry methodology for membrane lipid profiling through hydrophilic interaction liquid chromatography, J. Chromatogr. A. 1384 (2015) 44–52. doi:10.1016/j.chroma.2015.01.035.

[9] A. Fauland, H. Köfeler, M. Trötzmüller, A. Knopf, J. Hartler, A. Eberl, C. Chitraju, E. Lankmayr, F. Spener, A comprehensive method for lipid profiling by liquid chromatography-ion cyclotron resonance mass spectrometry, J. Lipid Res. 52 (2011) 2314–2322. doi:10.1194/jlr.D016550.

[10] M. Kliman, J.C. May, J.A. McLean, Lipid analysis and lipidomics by structurally selective ion mobility-mass spectrometry, Biochim. Biophys. Acta. 1811 (2011) 935–945. doi:10.1016/j.bbalip.2011.05.016.

[11] G. Paglia, P. Angel, J.P. Williams, K. Richardson, H.J. Olivos, J.W. Thompson, L. Menikarachchi, S. Lai, C. Walsh, A. Moseley, R.S. Plumb, D.F. Grant, B.O. Palsson, J. Langridge, S. Geromanos, G. Astarita, Ion mobility-derived collision cross section as an additional measure for lipid

fingerprinting and identification, Anal. Chem. 87 (2015) 1137–1144. doi:10.1021/ac503715v.

[12] G. Paglia, G. Astarita, Metabolomics and lipidomics using traveling-wave ion mobility mass spectrometry, Nat. Protoc. 12 (2017) 797–813. doi:10.1038/nprot.2017.013.

[13] M. Groessl, S. Graf, R. Knochenmuss, High resolution ion mobility-mass spectrometry for separation and identification of isomeric lipids, Analyst. 140 (2015) 6904–6911. doi:10.1039/C5AN00838G.

[14] A.P. Bowman, R.R. Abzalimov, A.A. Shvartsburg, Broad Separation of Isomeric Lipids by High-Resolution Differential Ion Mobility Spectrometry with Tandem Mass Spectrometry, J. Am. Soc. Mass Spectrom. 28 (2017) 1552–1561. doi:10.1007/s13361-017-1675-2.

[15] T. Baba, J.L. Campbell, J.C.Y. Le Blanc, P.R.S. Baker, Distinguishing Cis and Trans Isomers in Intact Complex Lipids Using Electron Impact Excitation of Ions from Organics Mass Spectrometry, Anal. Chem. 89 (2017) 7307–7315. doi:10.1021/acs.analchem.6b04734.

[16] T. Baba, J.L. Campbell, J.C.Y. Le Blanc, P.R.S. Baker, K. Ikeda, Quantitative structural multiclass lipidomics using differential mobility: electron impact excitation of ions from organics (EIEIO) mass spectrometry, J. Lipid Res. 59 (2018) 910–919. doi:10.1194/jlr.D083261.

[17] A.T. Maccarone, J. Duldig, T.W. Mitchell, S.J. Blanksby, E. Duchoslav, J.L. Campbell, Characterization of acyl chain position in unsaturated phosphatidylcholines using differential mobility-mass spectrometry, J. Lipid Res. 55 (2014) 1668–1677. doi:10.1194/jlr.M046995.

[18] T.P.I. Lintonen, P.R.S. Baker, M. Suoniemi, B.K. Ubhi, K.M. Koistinen, E. Duchoslav, J.L. Campbell, K. Ekroos, Differential mobility spectrometry-driven shotgun lipidomics, Anal. Chem. 86 (2014) 9662–9669. doi:10.1021/ac5021744.

[19] A.A. Shvartsburg, G. Isaac, N. Leveque, R.D. Smith, T.O. Metz, Separation and classification of lipids

using differential ion mobility spectrometry, J. Am. Soc. Mass Spectrom. 22 (2011) 1146–1155. doi:10.1007/s13361-011-0114-z.

[20] J.E. Keating, G.L. Glish, Dual Emitter Nano-Electrospray Ionization Coupled to Differential Ion Mobility Spectrometry-Mass Spectrometry for Shotgun Lipidomics, Anal. Chem. 90 (2018) 9117–9124. doi:10.1021/acs.analchem.8b01528.

[21] J.A.G. Roach, M.M. Mossoba, M.P. Yurawecz, J.K.G. Kramer, Chromatographic separation and identification of conjugated linoleic acid isomers, Anal. Chim. Acta. 465 (2002) 207–226. doi:10.1016/S0003-2670(02)00193-9.

[22] L.J. Morris, Separations of lipids by silver ion chromatography, J. Lipid Res. 7 (1966) 717–732.

[23] W.W. Christie, A stable silver loaded column for the separation of lipids by HPLC, J. High Resolut. Chromatogr. 10 (1987) 148–150. doi:10.1002/jhrc.1240100309.

[24] G. Dobson, W.W. Christue, B. Nikalovadamyanova, Silver ion chromatography of lipids and fatty-acids, J. Chromatogr. B. 671 (1995) 197–222. doi:10.1016/0378-4347(95)00157-E.

[25] B.B. Schneider, T.R. Covey, S.L. Coy, E. V Krylov, E.G. Nazarov, Planar differential mobility spectrometer as a pre-filter for atmospheric pressure ionization mass spectrometry, Int. J. Mass Spectrom. 298 (2010) 45–54. doi:10.1016/j.ijms.2010.01.006.

[26] B.B. Schneider, E.G. Nazarov, F. Londry, P. Vouros, T.R. Covey, Differential Mobility Spectrometry/Mass Spectrometry History, Theory, Design Optimization, Simulations, and Applications, Mass Spectrom. Rev. 35 (2016) 687–737. doi:10.1002/mas.21453.

[27] C. Liu, J.C.Y. Le Blanc, J. Shields, J.S. Janiszewski, C. Ieritano, G.F. Ye, G.F. Hawes, W.S. Hopkins, J.L. Campbell, Using differential mobility spectrometry to measure ion solvation: an examination of the roles of solvents and ionic structures in separating quinoline-based drugs, Analyst. 14 (2015)

6897–6903. doi:10.1039/C5AN00842E.

[28] C. Liu, J.C. Yves Le Blanc, B.B. Schneider, J. Shields, J.J. Federico, H. Zhang, J.G. Stroh, G.W. Kauffman, D.W. Kung, C. Ieritano, E. Shepherdson, M. Verbuyst, L. Melo, M. Hasan, D. Naser, J.S. Janiszewski, W.S. Hopkins, J.L. Campbell, Assessing Physicochemical Properties of Drug Molecules via Microsolvation Measurements with Differential Mobility Spectrometry, ACS Cent. Sci. 3 (2017) 101–109. doi:10.1021/acscentsci.6b00297.

[29] D.J. Wales, J.P.K. Doye, Global Optimization by Basin-Hopping and the Lowest Energy Structures of Lennard-Jones Clusters Containing up to 110 Atoms, J. Phys. Chem. A. 101 (1997) 5111–5116. doi:10.1021/jp970984n.

[30] C. Ieritano, P.J.J. Carr, M. Hasan, M. Burt, R.A. Marta, V. Steinmetz, E. Fillion, T.B. Mcmahon, W.S. Hopkins, The structures and properties of proton- and alkali-bound cysteine dimers, Phys. Chem. Chem. Phys. 18 (2016) 4704–4710. doi:10.1039/C5CP07414B.

[31] W.S. Hopkins, R.A. Marta, V. Steinmetz, T.B. McMahon, Mode-specific fragmentation of amino acid-containing clusters, Phys. Chem. Chem. Phys. 17 (2015) 28548–28555. doi:10.1039/C5CP03517A.

[32] M. Burt, K. Wilson, R. Marta, M. Hasan, W. Scott Hopkins, T. McMahon, Assessing the impact of anion–π effects on phenylalanine ion structures using IRMPD spectroscopy, Phys. Chem. Chem. Phys. 16 (2014) 24223–24234. doi:10.1039/C4CP03776F.

[33] C. Ieritano, J. Featherstone, P.J.J. Carr, R.A. Marta, E. Loire, T.B. McMahon, W.S. Hopkins, The structures and properties of anionic tryptophan complexes, Phys. Chem. Chem. Phys. 20 (2018) 26532–26541. doi:10.1039/C8CP04533J.

[34] M. J. Frisch, G. W. Trucks, H. B. Schlegel, G. E. Scuseria, M. A. Robb, J. R. Cheeseman, G. Scalmani,

B. V. Barone, G. Mennucci and A. Petersson, Gaussian 16, Revision A.03, Gaussian, Inc., Wallingford CT, 2016.

[35] W.D. Cornell, P. Cieplak, C.I. Bayly, I.R. Gould, K.M. Merz, D.M. Ferguson, D.C. Spellmeyer, T. Fox, J.W. Caldwell, P.A. Kollman, A second generation force field for the simulation of proteins, nucleic acids, and organic molecules, J. Am. Chem. Soc. 117 (1995) 5179–5197. doi:10.1021/ja00124a002.

[36] A.D. Becke, Density-Functional Exchange-Energy Approximation with Corrects Asymptotic-Behavior, Phys. Rev. A. 38 (1988) 3098–3100. doi:10.1103/PhysRevA.38.3098.

[37] C. Lee, W. Yang, R.G. Parr, Development of the Colle-Salvetti correlation-energy formula into a functional of the electron density, Phys. Rev. B. 37 (1988) 785–789. doi:10.1103/PhysRevB.37.785.

[38] C.M. Breneman, K.B. Wiberg, Determining atom-centered monopoles from molecular electrostatic potentials. The need for high sampling density in formamide conformational analysis, J. Comput. Chem. 11 (1990) 361–373. doi:10.1002/jcc.540110311.

[39] C.D. Michener, R.R. Sokal, A quantitative approach to a problem in classification, Evolution (N. Y). 11 (1957) 130–162.

[40] R.R. Sokal, C.D. Michener, A statistical method for evaluating systematic relationships, in: Univ. Kansas Sci. Bull., 1958: pp. 1409–1438.

[41] W. Fu, W.S. Hopkins, Applying Machine Learning to Vibrational Spectroscopy, J. Phys. Chem. A. 122 (2018) 167–171. doi:10.1021/acs.jpca.7b10303.

[42] R. Parthasarathi, J. Tian, A. Redondo, S. Gnanakaran, Quantum chemical study of carbohydrate-phospholipid interactions, J. Phys. Chem. A. 115 (2011) 12826–12840. doi:10.1021/jp204015j.

[43] J. Chai, M. Head-Gordon, Long-range corrected hybrid density functionals with improved

dispersion corrections, Phys. Chem. Chem. Phys. 10 (2008) 6615–6620. doi:10.1021/ct300715s.

[44] F. Weigend, R. Ahlrichs, {B}alanced Basis Sets of Split Valence, Triple Zeta Valence and Quadruple Zeta Valence Quality for {H} to {R}n: {D}esign and Assessment of Accuracy., Phys. Chem. Chem. Phys. 7 (2005) 3297–3305. doi:10.1039/b508541a.

[45] D. Andrae, U. Haeussermann, M. Dolg, H. Stoll, H. Preuss, Energy-adjusted ab initio pseudopotentials for the second and third row transition elements, Theor. Chim. Acta. 77 (1990) 123–141. doi:10.1007/BF01114537.

[46] U.C. Singh, P.A. Kollman, An approach to computing electrostatic charges for molecules, J. Comput. Chem. 5 (1984) 129–145. doi:10.1002/jcc.540050204.

[47] B.H. Besler, K.M. Merz, P.A. Kollman, Atomic charges derived from semiempirical methods, J. Comput. Chem. 11 (1990) 431–439. doi:10.1002/jcc.540110404.

[48] C. Ieritano, J. Crouse, J.L. Campbell, S. Hopkins, A parallelized molecular collision cross section package with optimized accuracy and efficiency, Analyst. 144 (2019) 1660–1670. doi:10.1039/C8AN02150C.

[49] E.F. Pettersen, T.D. Goddard, C.C. Huang, G.S. Couch, D.M. Greenblatt, E.C. Meng, T.E. Ferrin, UCSF Chimera - A visualization system for exploratory research and analysis, J. Comput. Chem. 25 (2004) 1605–1612. doi:10.1002/jcc.20084.

[50] A.A. Shvartsburg, M.F. Jarrold, An exact hard-spheres scattering model for the mobilities of polyatomic ions, Chem. Phys. Lett. 261 (1996) 86–91. doi:10.1016/0009-2614(96)00941-4.

[51] J. Yin, Y. Zhao, Hybrid QM / MM simulation of the hydration phenomena of dipalmitoylphosphatidylcholine headgroup, J. Colloid Interface Sci. 329 (2009) 410–415. doi:10.1016/j.jcis.2008.09.070.

[52] E. Mrázková, P. Hobza, M. Bohl, D.R. Gauger, W. Pohle, Hydration-Induced Changes of Structure and Vibrational Frequencies of Methylphosphocholine Studied as a Model of Biomembrane Lipids, J. Phys. Chem. B. 109 (2005) 15126–15134. doi:10.1021/jp051208f.

[53] W. Pohle, D.R. Gauger, M. Bohl, E. Mrázková, P. Hobza, Lipid Hydration: Headgroup CH Moieties Are Involved in Water Binding, Biopolymers. 74 (2004) 27–31. doi:10.1002/bip.20037.

[54] J.E. Kyle, X. Zhang, K.K. Weitz, M.E. Monroe, Y.M. Ibrahim, R.J. Moore, J. Cha, X. Sun, E.S. Lovelace, J. Wagoner, S.J. Polyak, T.O. Metz, S.K. Dey, R.D. Smith, K.E. Burnum-Johnson, E.S. Baker, Uncovering biologically significant lipid isomers with liquid chromatography, ion mobility spectrometry and mass spectrometry, Analyst. 141 (2016) 1649–1659. doi:10.1039/c5an02062j.

[55] W.S. Hopkins, Dynamic Clustering and Ion Microsolvation, in: W.A. Donald, J.S. Prell, D. Barcelò (Eds.), Adv. Ion Mobilty-Mass Spectrom. Fundam. Instrumentation, Appl., 83rd ed., Elsevier, 2019: pp. 83–118.